Design guidelines for efficient eutectic soldering onto low Tg polymeric multimode light waveguides

Meriem Ben Salah Ep Akin
Lutz Rissing
Elke Pichler

Electrical Engineering and Computer Sciences
University of California at Berkeley

Technical Report No. UCB/EECS-2014-52
http://www.eecs.berkeley.edu/Pubs/TechRpts/2014/EECS-2014-52.html

May 3, 2014

Acknowledgement

The authors gratefully acknowledge the financial support by Deutsche Forschungsgesellschaft (DFG) within the Collaborative Research Center “Transregio 123-Planar Optronic Systems.”

Design guidelines for efficient eutectic soldering onto low Tg polymeric multimode light waveguides

Meriem Akin, Lutz Rissing, Elke Pichler

Abstract

In this work, we conduct a numerical investigation of the structural feasibility of a flexible, monolithic and planar opto-electronic system based on low Tg polymers using ANSYS™. In particular, we explore the effectiveness of two eutectic compounds 52w.%In 48w.%Sn and 58w.%Bi 42w.%Sn to solder light sources and sinks to multimode light waveguides. First, we analyze the warpage of the optical structures due to eutectic soldering. Furthermore, we study the spectrum of mechanical stresses within the eutectic layer. Then, we investigate the possibility of roll-to-roll mass production. Finally, we establish design guidelines for decreasing the system warpage, and consequently preserving optical alignment, while complying with the ultimate shear strength of the eutectic material.

1. Related Work

Nowadays, inexpensive and flexible organic materials such as low glass transition temperature (Tg) polymers ([4], [5]) combined with high-throughput roll-to-roll (R2R) mass production ([1], [2], [3]) are increasingly gaining industrial value. Specifically, low-cost opto-electronic sensors ([6], [7]) can benefit from the use of the aforementioned strategies. Here, an opto-electronic sensor is assumed to include at least one electrically fed light source, one electrically fed light detector, a network of light waveguides and finally coupling structures to focus the light from and to light sources, light sinks and light waveguides.

While performance is a crucial factor for the success of polymeric opto-electronic sensors, monolithicity of the opto-electronic system remains a challenge. In particular, monolithicity is established once electronics, optics and opto-electronics are assembled on the very same substrate. Existing opto-electronic systems overcome the aforementioned challenge by discretizing the system and decoupling various mechanical, chemical and thermal limitations across the system. For instance, a flexible shear sensor, and a strain and pressure sensor based on opto-electronics were demonstrated in [8] and [9] respectively, where opto-electronic components and optics were manufactured on different substrates and materials, and subsequently integrated. While performance, which is particularly secured by optical alignment, was ensured, a R2R manufacturing approach was clearly impaired due to the lack of monolithicity. In [10], while the light source and sink were integrated onto one single flexible platform, light waveguides were not realized.

In order to guarantee a flexible and monolithic opto-electronic sensor, optical alignment has to be given. Assuming that the light sources and sinks are surface mount devices, a surface mount technology has to be established thoroughly. Clearly, classical high-temperature soldering and wire-bonding of opto-electronic components fail. Accordingly, surface mount methods of opto-electronic components need to be adjusted to the optical tolerances. For instance, although planarity of the system was hindered, an out-of-plane optical interface was used to connect an already packaged opto-electronic component to a printed circuit board, which houses the light waveguides [11]. Therefore, warpage of the printed circuit board due to packaging of the opto-electronic component was substantially minimized. Furthermore, continuous active alignment of opto-electronic components during a soldering cycle, while the opto-electronic components are in operation, helps meeting the required optical tolerances [12]. Nonetheless, costs of active alignment need not to be neglected. In this case, light couplers such as micro-mirrors definitely assist passive alignment [13].

Nomenclature

3D	three dimensional
Bi	Bismuth
BiSn	58w.%Bi 42w.%Sn
CTE	coefficient of thermal expansion
Cu	Copper
GaAs	Gallium Arsenide
In	Indium
InSn	52w.%In 48w.%Sn

PET	Polyethylene Terephthalate
PMMA	Poly(methyl methacrylate)
R2R	roll-to-roll
Sn	Tin
Tg	glass transition temperature
w.%	weight percentage

Here, we present a computational study investigating the thermo-mechanical feasibility of a flexible, monolithic and planar opto-electronic system based on a low Tg polymeric substrate. Notably, the system is to be manufactured using a R2R process. Besides, light sources and sinks are to be surface mounted by means of a low temperature soldering process according to [30]. In particular, we establish design guidelines for decreasing the system warpage, and therefore preserving optical alignment and mechanical reliability.

2. Opto-electronic system: geometry and materials

We research an opto-electronic system (Figure 1) that employs a hybrid selection of materials. Here, Poly(methyl methacrylate), having a Young's modulus of 1950 MPa, a Poisson's ratio of 0.375 and a Tg of 105 deg. C [14], serves as the substrate material. Then, multimode light waveguides made of Polyethylene Terephthalate are embedded in the substrate, which are characterized by a Young's modulus of 3780 MPa [18], a Poisson's ratio of 0.405 [19] and a Tg of 71 deg. C [20]. In terms of optical properties, Poly(methyl methacrylate) (PMMA) has an optical refractive index of n=1.489 at a wavelength of 632.8 nm [15], while Polyethylene Terephthalate (PET) has a refractive index of n=1.636 at the same wavelength [17]. Next, embedded couple structures, in particular grating structures, enable light reception and emission from-and-to substrate. Further, Copper (Cu) interconnects establish a metallic interface between substrate, light sources, and sinks. Here, Cu has a Young's modulus of 130 GPa and a Poisson's ratio of 0.34 [16]. Lastly, three dimensional (3D) light emitting diode and photodiode that are based on Gallium Arsenide (GaAs) are surface mounted to the surface of the polymeric substrate employing a low temperature eutectic solder. In this work, we assume that Gallium Arsenide has a Young's modulus of 85 GPa and a Poisson's ratio of 0.31 [22]. In addition, we explore the effectiveness of two commercially conventional eutectic compounds 52w.%In 48w.%Sn (InSn) and 58w.%Bi 42w.%Sn (BiSn) as a soldering layer. While InSn melts at 118 deg. C, BiSn liquefies at 138 deg. C. Moreover, the Young's modulus of InSn and BiSn are assumed to be 19.5 GPa and 43 GPa [23], and the Poisson's ratio of InSn and BiSn are 0.36 [25] and 0.35 [24] respectively.

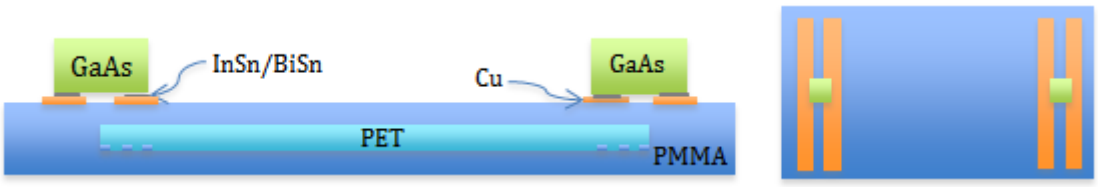

Figure 1: Opto-electronic system (Right: top view; Left: cross section view; Note: views do not have the same dimensional scale)

Coefficients of thermal expansion (CTEs) of the materials of the system are key properties for the realization of optical alignment. CTEs of GaAs and Copper are taken to be 6.4 ppm/K [21] and 16.6 ppm/K [26] respectively, and constant over the soldering cycle due to their rigid nature and low soldering temperature. CTEs of the remaining materials are experimentally determined continuously over the soldering cycle. Using an optical dilatometer, material samples of the size of 24 mm x 12mm were heated starting at room temperature to a maximum of 130 deg. C. while gradually increasing the temperature with a ramp of 1 K/min. Notably, the temperatures at which CTEs were measured were maintained for 20 minutes duration. Analogously, the samples were cooled down. Accordingly, CTEs of the various materials of the opto-electronic system are depicted in Figure 2.. Additionally, the ultimate shear strengths of the bearing layers InSn, BiSn and Cu are critical for the reliability of the system. On that account, the shear strength of InSn and BiSn are assumed to be 11.2 MPa and 3.4 MPa respectively [27].

The overall size of the system is 16 mm x 20 mm, while the light waveguide length is 16 mm and the PMMA substrate thickness is 0.2 mm. Furthermore, the surface area of the opto-electronic components attached to the PMMA substrate is 0.1 mm x 0.1 mm. Besides, each Cu pad has a thickness of 0.02 mm. A solder joint has a

cross section of 0.025 mm x 0.1 mm. The diffraction grating has a period of 0.025 mm, a thickness of 0.02 mm and the same width as the PET waveguide. Then, the waveguide has a quadratic cross section. Subsequently, the size of the waveguide cross section, the thickness of the opto-electronic components and that of the solder layer, as well as the width and length of the Cu pads will be varied and investigated.

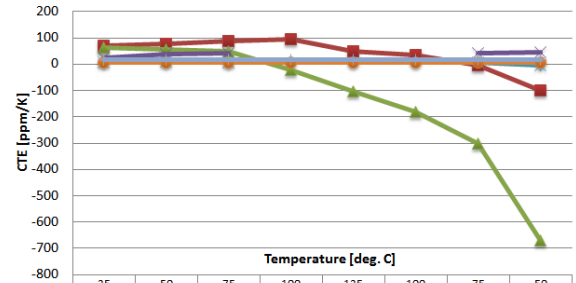

	25	50	75	100	125	100	75	50
PMMA	71	76	88	96	50	35	-4,15	-100
PET	65	58	51	-21	-104	-180	-303	-670
InSn	23	39	42				42	47
BiSn	6	9	7				8	-3
GaAs	6,4	6,4	6,4	6,4	6,4	6,4	6,4	6,4
Cu	16,6	16,6	16,6	16,6	16,6	16,6	16,6	16,6

Figure 2: Development of CTEs of the system materials over a soldering cycle

3. Theoretical Pre-Analysis

Adopting the theory of Timoshenko on a bi-layer thermostat [28], soldering aftereffects on two decoupled subsystems: (a) substrate-waveguide and (b) component-substrate are investigated for both InSn and BiSn variations. In particular, we use the theory of Timoshenko to analyze the opto-electronic system due to thermal shrinkage after soldering and mismatches in CTEs. It is to be noted that Timoshenko assumes the layers of the thermostat to be of the same length. Therefore, both of the subsystems are focused on the actual contact region between the layers, i.e. the substrate-waveguide subsystem is 16 mm long, and the component-substrate subsystem is 0.1 mm long. First, we study the effect of the waveguide thickness on the warpage of the substrate-waveguide subsystem and on the interfacial load at the fibers of the bearing surface between substrate and waveguide. Here, the substrate-waveguide subsystem does not include the opto-electronic component. Then, we analyze the implication of thinning of the opto-electronic component on the warpage of the component-substrate subsystem and on the interfacial load at the bearing surface between substrate and component. Notably, the waveguide is not part of the component-substrate subsystem. Unless otherwise stated, dimensions and material properties listed in the previous section are adopted for this analysis.

In terms of the substrate-waveguide subsystem, multimode waveguides having sizes between 0.01 mm and 0.1 mm exhibit large warpages, but small interfacial loads (Figure 3). Clearly, a difference of 6 ppm/K in thermal expansion between substrate and waveguide in addition to the low rigidity of the polymers is the cause for large warpages. Nevertheless, significant reduction of warpages is first observed for single mode waveguides with sizes less than or equal to 0.01 mm. Mainly, the low melting temperature of InSn leads to a less deformed and a less stressed system. Interestingly, the BiSn-system is noted to deform less than the InSn-system does in the case of multimode waveguides due to the higher difference between melting temperature of BiSn and room temperature, and due to low thickness ratio between substrate and waveguide. Finally, the warpage of the substrate-waveguide system is characterized by a smiling shape.

Thinning of 3D components is a common practice for ensuring planarity and flexibility of the assembled system [29]. Here, thinning of the 3D opto-electronic component leads to an increasing frowning warpage. However, interfacial loads between the component and the substrate decrease due to the loss in rigid volume. Nonetheless, warpage and interfacial loads remain substantial despite extreme thinning of the component, mainly due to a mismatch of 64 ppm/K in thermal expansion. As expected, lower soldering temperatures, and so the choice of InSn, lead to a less stressed and less deformed system.

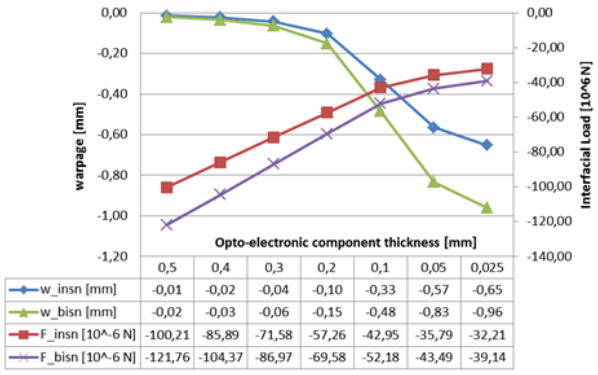

	0,5	0,4	0,3	0,2	0,1	0,05	0,025
w_insn [mm]	-0,01	-0,02	-0,04	-0,10	-0,33	-0,57	-0,65
w_bisn [mm]	-0,02	-0,03	-0,06	-0,15	-0,48	-0,83	-0,96
F_insn [10^-6 N]	-100,21	-85,89	-71,58	-57,26	-42,95	-35,79	-32,21
F_bisn [10^-6 N]	-121,76	-104,37	-86,97	-69,58	-52,18	-43,49	-39,14

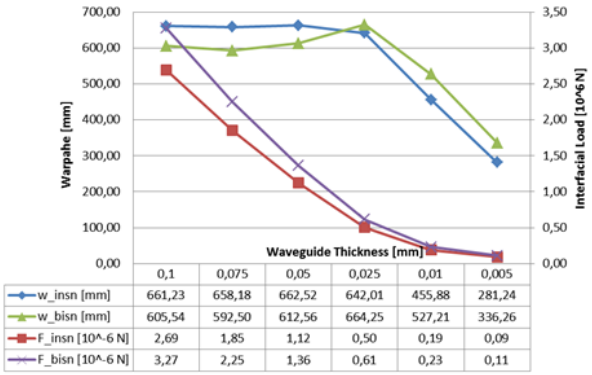

	0,1	0,075	0,05	0,025	0,01	0,005
w_insn [mm]	661,23	658,18	662,52	642,01	455,88	281,24
w_bisn [mm]	605,54	592,50	612,56	664,25	527,21	336,26
F_insn [10^-6 N]	2,69	1,85	1,12	0,50	0,19	0,09
F_bisn [10^-6 N]	3,27	2,25	1,36	0,61	0,23	0,11

Figure 3: Right: Effect of waveguide thickness on substrate warpage and interfacial load between substrate and waveguide, Left: Effect of thickness of opto-electronic component on substrate warpage and interfacial load between substrate and waveguide

4. Computational Analysis

In order to investigate the structural reliability of the entire opto-electronic system, a numerical investigation becomes necessary. In particular, thermal shrinkage due to cooling after soldering is analyzed. We use ANSYS™ to model the system described in section 2. Here, we assume that the light sources and sinks are fully soldered to the interconnects, i.e., the bottom surface of the opto-electronic component is completely coated by the eutectic solder. Moreover, cooling is modeled as a global thermal body load, whereas the soldering temperature is assumed to be stress-free. Besides, materials are assumed to behave constitutively elastic while cooling down from soldering temperature to room temperature. Hence, the 3D finite element type solid185 is used. For numerical convergence purposes, the size of the numerical model results in about 195000 degrees of freedom. We employ a primary model, such that Cu pads are of 0.15 mm thickness, solder is of 0.025 mm thickness, waveguide is of 0.1 mm thickness, opto-electronic components is of 0.025 mm thickness. Besides, the primary model is assumed to have the waveguide to be centric to the PMMA substrate. Based on the primary model, we investigate the effect of assembly, design symmetry, position on the rolled-out polymer film, solder amount, and thickness and size of interconnects on the solderability of the opto-electronic system. By imposing coupled degrees of freedom to the boundary of the system unit, the position on the rolled-out polymer is modeled. In the case of a unit placed in the middle of an open roll, all four edges have coupled degrees of freedom, whereas for the unit placed at the edge of an open roll, three edges have coupled degrees of freedom and the open edge is not constrained. Finally, the system is ensured to be statically determinate by constraining vertical displacement of one corner.

4.1. Position on roll

We analyze the effect of the position of a system unit on a rolled-out polymer film on the waveguide warpage and the spectrum of shear stresses within the solder joint (Figure 4). In particular, units positioned on the edge of the rolled-out polymer film exhibit larger waveguide warpages. However, the shear stresses do not depend on the system position. Even though mechanically not less reliable, units on the edge are optically less efficient, and

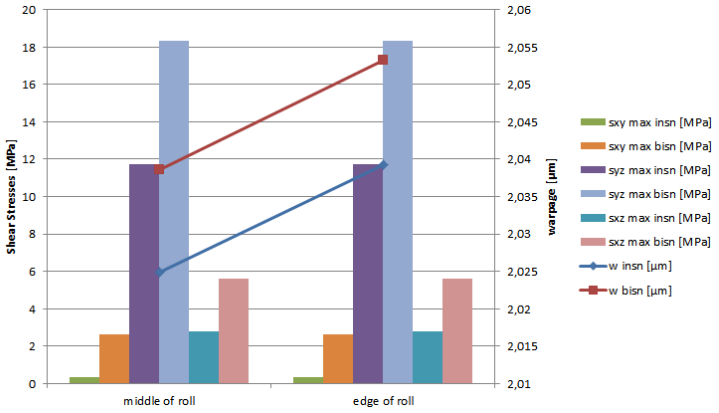

Figure 4: Effect of position on roll on waveguide warpage and shear stresses within the solder joint

might therefore need to be discarded. Also, we confirm that units soldered with InSn are less deformed and less stressed than units soldered with BiSn both on the middle and edge of the roll. More importantly, shear stresses within the BiSn solder are extremely beyond the ultimate shear strength of BiSn. Due to the low ductility of the material, BiSn is not recommended for manufacturing the proposed opto-electronic system.

4.2. System assembly

As depicted in Figure 5, the warpage of the opto-electronic system is mostly due to the choice of Copper as a material for the interconnects. It is noted that the waveguide warpage of the substrate-waveguide-subsystem is nearly doubled when including the interconnects to the subsystem. However, the solder and opto-electronic component material induce a negligible increase in waveguide warpage of about 0.5%. Consequently, it is

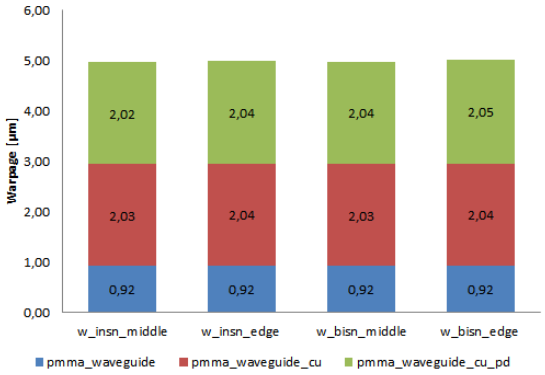

Figure 5: Warpage due to soldering for three subsystems: substrate-waveguide, substrate-waveguide-interconnects and substrate-waveguide-interconnects-solder-component

recommended to choose a different material for the interconnects with a closer CTE to that of the polymeric materials. In the computational model, the waveguide is completely embedded in the substrate, and so the substrate-waveguide subsystem exhibits lower warpages than calculated by theory in section 3.

4.3. Symmetry in design

We investigate the effect of symmetry of the design on the waveguide warpage and the shear stresses within the solder joint by introducing an offset of 0.5 mm to the center of the waveguide with respect to the PMMA substrate. Remarkably, asymmetry leads to an increase of up to 100% in waveguide warpage depending on position of system unit and solder material. While for symmetric designs, most of the shear stress components are partitioned equally between light source and sink, a slight imbalance occurs when symmetry of design is not

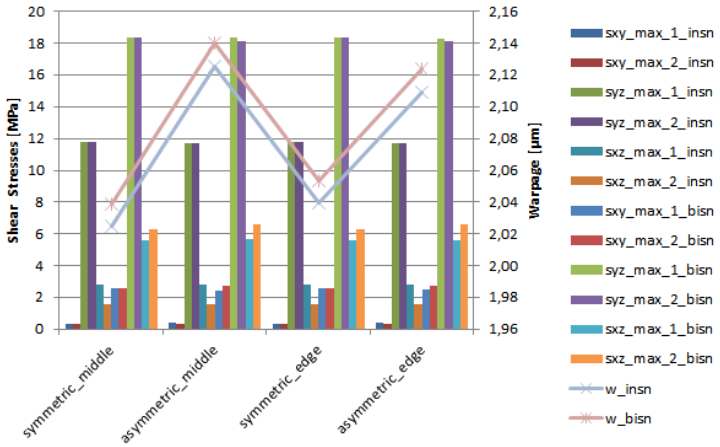

Figure 6: Effect of symmetry on waveguide warpage and shear stresses within solder joints

fulfilled (Figure 6). Moreover, the shear stress components slightly increase in value. Therefore, a symmetric design is beneficial for decreasing warpage and shear stresses, and should be obtained whenever possible.

4.4. Solder amount

The effect of the solder amount on the waveguide warpage and spectrum of shear stresses within the solder is studied. As depicted in Figure 7, a trade-off between monitoring warpage and stresses occurs. While decreasing the solder thickness minimizes shear stresses within the InSn solder, the waveguide warpage increases. Nevertheless, a solder thickness of less than 15 µm turns the system into lower mechanical reliability and, simultaneously, inefficient optical alignment. In the case of solder thickness of 50 µm, the shear stresses are below the ultimate shear strength of InSn, and lowest waveguide warpage is recorded. Nevertheless, only a moderate 0.5% decrease in waveguide warpage is achieved with this approach.

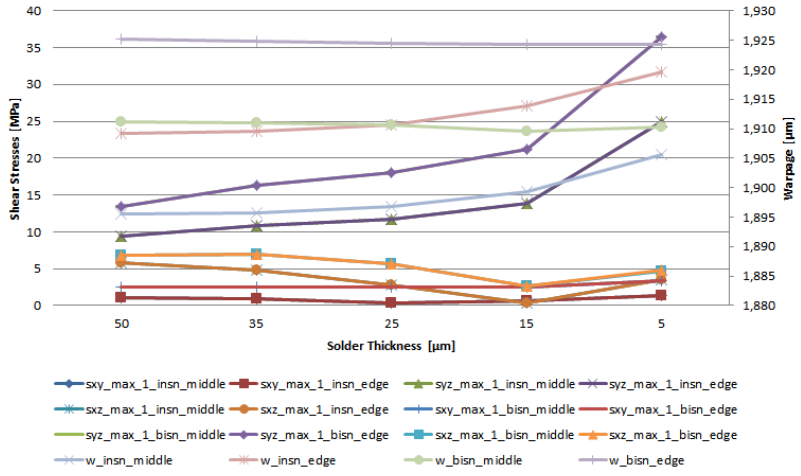

Figure 7: Effect of solder thickness on waveguide warpage and shear stresses within solder joints

4.5. Thickness and size of interconnects/contacting pads

While the material of interconnects was shown in section 4.2 to affect optical alignment remarkably, waveguide warpage can still be monitored by adjusting the thickness of the interconnects as well as the edge size of the contacting pad. As shown in Figure 8, narrower and thinner interconnects lead to a less deformed system.

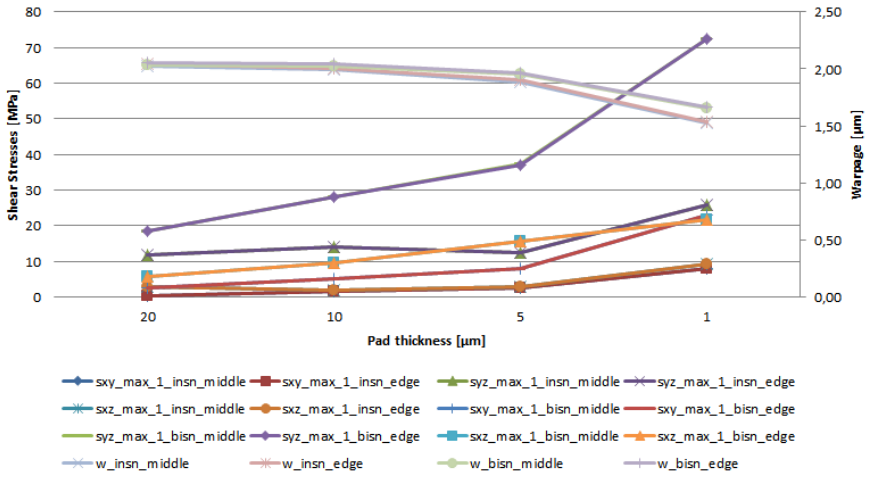

Figure 8: Effect of interconnects thickness and size on warpage and shear stresses within solder

Notably, thinner interconnects are subject to larger shear stresses. Therefore, the interconnects should not be

thinner than 5 µm in order to comply with the ultimate shear strength of InSn. Moreover, it is important to maintain a substantial thickness of the interconnects in order to enable soldering.

Conclusion

In this work, we studied the feasibility of a planar and monolithic opto-electronic system for a R2R mass production based on theoretical and numerical models. We developed design guidelines to facilitate eutectic soldering of opto-electronic components onto low Tg polymers while being accurately aligned to light waveguides. For the proposed system, it is concluded that InSn is better than BiSn as a eutectic solder due to lower melting temperature and higher ductility. Besides, Cu is not the ideal material for interconnects onto low Tg polymers due to large mismatches in thermal expansion. Moreover, system units positioned in the middle of the rolled-out polymer are expected to exhibit less light loss due to lower warpage. In order to reduce the warpage of the light waveguide and comply with the ultimate shear strength of InSn, we deduce four main design guidelines: (1) thinner interconnects, (2) narrower interconnects, (3) thicker solder and (4) symmetric design.

Acknowledgements

The authors gratefully acknowledge the financial support by Deutsche Forschungsgesellschaft (DFG) within the Collaborative Research Center “Transregio 123-Planar Optronic Systems.”

References

[1] Frederik C. Krebs, Thomas Tromhold, Mikkel Jorgensen. Upscaling of polymer solar cell fabrication using full roll-to-roll processing. *Nanoscale* 2010; **2**: 873-886.

[2] Se Hyun Ahn, L. Jay Guo. Large-area roll-to-roll and roll-to-plate nanoimprint lithography: a step toward high-throughput application of continuous naoimprinting. *ACS Nano* 2009, **3(8)**: 2304-2310.

[3] Nieves Espinosa, Rafael Garcia-Valverde, Antonio Urbina, Frederik C. Krebs. A life cycle analysis of polymer solar cell moduls prepared using roll-to-roll methods under ambient conditions. *Solar Energy Materials and Solar Cells* 2011, **95(5)**: 1293-1302

[4] David Voss. Cheap and cheerful circuits, *Nature* 2000, **407:**442-444

[5] Sean E. Shaheen, David S. Ginley, Ghassan E. Jabbour. Organic-based photovoltaics: toward low-cost power generation. MRS Bulletin 2005, **30 (1)**: 10-19

[6] Louay Eldada, Lawrence W. Shacklette. Advances in Polymer Integrated Optics, *IEEE Journal of selected topics in quantum electronics* 2000, **6(1)**: 54-67

[7] Louay Eldada. Polymer integrated optics: promise versus practicality, Poceedings of SPIE 2002, **4642**: 11-22

[8] J. Missine, E. Bosman, B. Van Hoe, G. Van Steenberge, S. Khalathimekkad, P. Van Daele, J. Vanfleteren. Flexible shear sensor based on embedded optoelectronic components, IEEE Photonics Technology Letters 2011, **23(12)**: 771-772

[9] X. Chen, C. Zhang, B. Van Hoe, D. J. Webb, K. Kalli, G. Van Steenberge, G-D. Peng. Photonic skin for pressure and strain sensing, Proceedings of SPIE 2010, 7726: 772604-1:9

[10] J. A. C. Patterson, D. G. Mcllwraith, G.-Z. Yang. A flexible, low noise reflective PPG sensor for the ear-worn heat rate monitoring, Sixth national workshop on Wearable and Implantable Body Sensor Networks 2009, **16**: 286-291

[11] Y. Ishii, S. Koike, Y. Arai, Y. Ando. SMT-Compatible large tolerance “OptoBump” interface for interchip optical interconnections, IEEE Transactions on Advanced Packaging 2003, **26 (2):** 122-127

[12] L. Stauffer, A. Wursch, B. Gachter, K. Siercks, I. Verettas, S. Rossopoulos, R. Clavel. A surface-mounted device assembly technique for small optics based on laser reflow soldering, Optics and Lasers in Engineering 2005, **43(3-5)**: 365-372

[13] T. Satoh, A. Ichimura, O. Mikami, S. Tomaru, M. Hikita, T. Uchida. Coupling of spot-size converted laser diode to polymeric waveguide with 45-degree micro-reflection mirror for optical surface mount technology, 2nd Symposium IEMT/IMC 1998, 114-117

[14] MIT Material property database, http://www.mit.edu/~6.777/matprops/pmma.htm

[15] T. Ishigure, E. Nihei, Y. Koike. Optimum reflective-index profile of the graded-index polymer optical fiber, toward gigbit data links, Applied Optics 1996, **35(12):** 2048-2053

[16] MIT Material property database, http://www.mit.edu/~6.777/matprops/copper.htm

[17] Filmetrics Refractive index database, http://www.filmetrics.com/refractive-index-database/PET/Estar-Melinex-Mylar

[18] C. Reynaud, F. Sommer, C. Quet, N. El Bounia, T. M. Duc. Quantitative determination of Young’s modulus on a biphase polymer system using atomic force microscopy

[19] I. Wilson, N. H. Ladizesky, I.M. Ward. The determination of Poisson’s ratio and extensional modulus for polyethylene terephtalate sheets by an optical technique, Journal of Materials Sciences 1976, **11:** 2177-2180

[20] C. E. Wikes. PVC Handbook 2005, Hanser Verlag.

[21] K. Hjort, J. Soderkvist, J-A. Schweitz. Gallium arsenide as a mechanical material, Journal of Michromechanics and Microengineering 1994, **4(1)**:1-13

[22] Janis Material property database
http://www.janis.com/Libraries/Window_Transmissions/GalliumArsenide_GaAs_TransmissionCurveDataSheet.sflb.ashx

[23] M. Abtew, G. Selvaduray. Lead-free solders for surface mount technology applications (Part2), Chip Scale Review 1998

[24] H. Tanaka, L. F. Qun, O. Munekata, T. Taguchi, T. Nashita. Elastic properties of Sn-based Pb-free alloys determined by ultrasonic pulse echo method, Materials Transactions 2005, **46(6)**: 1271-1273

[25] J. Lau, Z. Mei, S. Pang, C. Amsden, J. Rayner. Creep analysis and thermal-fatigue life prediction of the lead-free solder sealing ring of a photonic switch, Journal of Electronic Packaging 2002, **124(4)**:403-410

[26] T. Rubin, H. W. Altman, H. L. Johnston. Coefficients of thermal expansion of solids at low temperatures. I. The thermal expansion of Copper from 15 to 300 K, Journal of American Chemical Society 1954, **76(21)**: 5289-5293

[27] Indium Corporation solder alloy guide, http://www.indium.com/solder-alloy-guide/

[28] S. Timoshenko. Analysis of Bi-metal Thermostats, Jounal of the Optical Society of America 1925, **11(3):**233-255

[29] C. Banda, R. Johnson, T. Zhang, Z. Hou, H. Charles. Flip chip assembly of thinned silicon die on flex substrates, IEEE Transactions on Electronics Packaging Manufacturing 2008, **31(1):**1-8

[30] M. Ben-Salah Akin, L. Rissing, W. Heumann. Enabling Eutectic Soldering of 3D Opto-Electronics onto Low Tg Flexible Polymers, Proceedings of 64th IEEE Electronic Components and Technology Conference 2014.